Published in final edited form as:
J Phys Chem B. 2011 December 29; 115(51): 15271–15279. doi:10.1021/jp209543c.

Interaction of melittin peptides with perfluorocarbon nanoemulsion particles

Sun-Joo Lee[1], **Paul H. Schlesinger**[2], **Samuel A. Wickline**[3], **Gregory M. Lanza**[4], and **Nathan A. Baker**[5]

[1]Department of Biochemistry and Molecular Biophysics, Center for Computational Biology, Washington University in St. Louis

[2]Department of Cell Biology and Physiology, Washington University in St. Louis

[3]Department of Medicine, Washington University in St. Louis

[4]Department of Medicine, Washington University in St. Louis

Abstract

Melittin, an anti-microbial peptide, forms pores in biological membranes and triggers cell death. Therefore it has potential as an anti-cancer therapy. However, until recently, the therapeutic application of melittin has been impractical because a suitable platform for delivery was not available. Recently, we showed that phospholipid stabilized perfluorooctylbromide- based nanoemulsion particles (PFOB-NEPs) were resistant to destruction by melittin and enabled specific delivery of melittin to tumor cells, killing them and reducing tumor growth. Earlier prior work also showed that melittin adsorbed onto the stabilizing phospholipid monolayer of PFOB-NEP but did not disrupt the phospholipid monolayer or produce “cracking” of the PFOB-NEPs. The present work identifies the important structural motifs for melittin binding to PFOB-NEPs through a series of atomistic molecular dynamics simulations. The conformational ensemble of melittin bound to PFOB-NEP lipid monolayer was compared to structure from a control simulation of melittin bound to a lipid bilayer to identify several differences in melittin-lipid interactions between the two systems. First, melittin was deeply buried in the hydrophobic tail region of bilayer, while its depth was attenuated in the PFOB-NEP monolayer. Second, a helical conformation was the major secondary structure in the bilayer, but the fraction of helix was reduced in the PFOB-NEP. Finally, the overall pattern for the direct interaction of melittin with surrounding lipids was similar between liposome and PFOB-NEP, but the level of interaction was slightly decreased in the PFOB-NEP. These results suggest that melittin interacts with the monolayer of PFOB-NEP in a way that is similar way to its interaction with bilayers but that deeper penetration into the hydrophobic interior is inhibited.

Keywords

Perfluorocarbon; nanoemulsions; melittin; molecular dynamics

Introduction

Nanoemulsion particles (NEPs) with perfluorocarbon (PFC) cores have shown great potential in delivering a wide range of therapeutic molecules to target cells.[1] PFCs are strongly hydrophobic and form nanoscale emulsions when mixed with water under strong

[5]To whom correspondence should be addressed. Pacific Northwest National Laboratory. nathan.baker@pnl.gov.

shear force.[2] Biomedical NEPs are often formulated with phospholipid surfactants that form monolayers enclosing and stabilizing the PFC droplets. PFCs are well known for their biological compatibility and clinical safety,[3] with years of demonstrated success as blood substitutes and in other applications.[4]

Recent efforts have focused on the use of PFC NEPs as platforms to specifically deliver melittin, an antimicrobial peptide (AMP), to cancer cells.[5] When targeted specifically to tumor cells, AMPs have shown promise as anti-cancer therapeutics.[5–6] Soman *et al*. demonstrated that melittin could be stably bound to PFC NEPs without disruption of NEP morphology or destabilization of the PFC emulsion.[5] Furthermore, they showed that NEP-bound melittin retains biological activity: the bound AMP can lyse liposomes and induce apoptosis *in vitro* and significantly reduce tumor size in *in vivo* mouse studies. Employing PFC NEPs has resolved many of the difficulties that previously prevented clinical applications of AMPs such as melittin in two ways: first, premature melittin degradation is prevented by limited protease access to peptides associated with the emulsifying phospholipid monolayer;[5b] second, the non-specific cytolytic activity can be directed to tumor cells by targeting the NEPs with tumor-cell-specific ligands on their surface.[5b]

Methods

Simulations

Initial structures—Melittin was studied in two model systems (see Figure 1): a planar model of a PFOB-NEP interface and a planar palmitoyl-oleoyl-phosphatidylcholine POPC bilayer. The initial planar PFOB-NEP interface model in the absence of melittin was prepared as described in previous work[7] with 1310 PFOB molecules sandwiched between two POPC monolayers comprising 64 lipids each. The entire system was surrounded by 11678 water molecules. Throughout the paper, this system will be referred to as “PFOB-NEP”. The initial planar POPC bilayer comprised 128 POPC lipids and 7714 water molecules. This system will be referred to as “control”.

To prepare the PFOB-NEP system, a single melittin peptide was inserted into each POPC monolayer to the mean depth of the glycerol groups (see Figure 1).[8] The peptide was inserted so that its non-polar residues faced the hydrophobic interior while its polar residues faced the NEP-water interface. POPC lipids that significantly overlapped with the inserted melittin peptides were deleted, leaving 55 POPC lipids remaining in each monolayer of the PFOB-NEP. A lipid:melittin ratio of 55:1 is less than the maximal concentration that melittin can interact with the PFOB-NEP monolayer but higher than the critical concentration of 100:1 required to exhibit cytolytic activity of the peptide in zwitterionic bilayer membranes.[8b],[9] No PFOB molecules had direct contact with the inserted melittin peptides and hence none of them were deleted. The NEP system was solvated by adding 18,959 water molecules. To neutralize the +5 formal charge of each melittin peptide, 10 randomly chosen water molecules were replaced by chloride ions. The hydration level of the system was over 90 water molecules per lipid, which ensured complete solvation. The dimensions of the system were 6.0 nm by 6.9 nm by 24.8 nm along the x, y, and z directions, respectively.

To prepare the control system, the initial planar POPC bilayer was duplicated along the x and y directions so that the duplicated bilayer contained enough POPC lipids per inserted peptide to allow a parallel orientation of the peptide along the membrane surface. After the lipids that significantly overlapped with the inserted melittin peptides were deleted, the lipids at the boundary of the bilayer were deleted to obtain a final ratio of 100:1 lipid:melittin in each monolayer. To solvate the POPC bilayer, 9,984 water molecules were added and 10 randomly chosen water molecules were replaced by chloride ions. A hydration

level of 90 water molecules per lipid was achieved. The dimensions of the system were 8.3 nm by 8.7 nm by 12.0 nm along the x, y, and z directions, respectively.

Force field parameters—PFOB was modeled with the force field parameters previously developed by Lee et al[7]. POPC was modeled with the united atom force field parameters optimized by Berger et al.[10] and Chiu et al.[11] The successful combination of the PFOB and POPC parameters was demonstrated in our previous work[7]. Water was modeled with the simple point charge SPC model[12] for compatibility with the Berger et al lipid parameter set. The melittin peptides used in these simulations were modeled with the OPLS-AA force field.[13] Mixing between the Berger lipid model and the OPLS-AA protein force field was performed using the half-epsilon pair-list approach as discussed and successfully applied in previous reports.[7, 14]

Simulation parameters—Molecular dynamics simulations and analyses of the trajectory were performed with GROMACS version 4.0.[15] The starting structures were subjected to previously described equilibration procedures.[16] First, an energy minimization was performed using a steepest descent method and the system was then gradually heated from 50 K to 303 K through a series of short molecular dynamics (MD) simulations. After the system reached the production temperature of 303 K, the MD simulation was continued for at least 300 ns of production simulation. Cutoffs for LJ interaction and for direct space for electrostatic interactions were set at 1.0 nm. The particle-mesh Ewald method,[17] with conducting boundary conditions, was used for long-range electrostatic interactions. The simulations were performed in an isobaric-isothermal ensemble (NpT) using the Parrinello-Rahman barostat[18] with 2 ps coupling time at 1 bar. The pressure coupling type varied depending on the systems: isotropic pressure coupling was used for simulations of bulk solutions, semi-isotropic for simulations of PFOB-NEP interface and POPC bilayer systems, and anisotropic for the simulation of melittin bound membranes. A Nosé-Hoover thermostat[19] with 0.5 ps coupling frequency was applied to each molecule type separately. Hydrogen atoms bonded to heavy atoms were constrained with the LINCS algorithm,[20] allowing a 2 fs time step to be used. To enhance the statistical significance of results, two and three replica simulations of melittin bound PFOB-NEP and control POPC bilayer systems were performed respectively for 300 ns. Initial velocities were randomly assigned from different Maxwell distributions for each simulation.

Analysis

To perform statistical analysis, each trajectory was divided into small blocks, with the block size chosen based on the standard error so that each block was independent of the others.[21] The standard error $\varepsilon(f, n)$ in observable f for a block of length n was calculated according to the formula

$$\varepsilon(f,n)=\sigma M^{1/2}$$

where σ is the standard deviation and M is the number of blocks in the simulation. When the block size is large enough; *i.e.*, much greater than the correlation time of an observable, the standard errors become independent of the block size and the true standard error is obtained. The block size for sub-sampling was determined by the value of n where $\varepsilon(f, n)$ for observable f reached a plateau. When observables were calculated for each monolayer separately, the results from each monolayer were combined and the number of independent blocks was doubled.

Results

Equilibration and subsampling

The total membrane area was used to assess the equilibration and the sizes of statistically independent subsamples. Substantial drift was only detected in one of the POPC "control" bilayer simulation (see Supplementary Figure 1). To remove this initial drift, the first 100 ns of trajectory were discarded from all simulations. The evolution of total membrane area of the remaining 200 ns-long trajectories was used to determine the independent subsample size as introduced in the Analysis section. A block size of ≥40 ns resulted in a plateau of standard errors in all five simulations (see Supplementary Figure 2). Therefore, a block size of 40 ns was applied, which generated five independent sub-samples for each simulation. Subsamples from each replica simulation were combined in 10 independent subsamples for the PFOB-NEP and 15 for the control system respectively. When the observables were computed for each monolayer, then the number of subsamples was doubled to 20 for the PFOB-NEP and 30 for the control.

Melittin secondary structure

Many AMPs undergo significant structural transitions when binding to membrane environments,[8a, 22] indicating the important role of the membrane environment for the structural properties of these peptides. Therefore, we assessed whether differences between the monolayer environment of the PFOB-NEP and the bilayer environment of the POPC Control result in differences in the bound melittin conformation. Using the DSSP algorithm[23], melittin secondary structures were categorized into six different conformations: random-coil, bend, turn, α-helix, 5-helix, and 3–10 helix. The fractions of each conformation adopted were determined for each melittin residue (see Figure 2).

The secondary structure of the membrane bound melittin was characterized by unstructured termini and structured internal residues. Helical conformations were pronounced in the structured region. In both systems, two major helical regions (residue 6-LKVLTTGLP-14 and residue 17-ISWIKRK-23) were separated at 15-AL-16 because of the kink generated by a proline residue. The first region was named "N-terminal helical region," and the second was named "C-terminal helical region."

Melittin bound to the monolayer of PFOB-NEP exhibited structural differences from the control systems. First, the total helical content of 11.4 (± 1.6) was smaller than 13.8 (± 1.5) in the control. Second, while the secondary structure profiles of the C-terminal helical segment were similar between the systems, the N-terminal helical segments were substantially different. Overall helical content was substantially lower because of the occurrence of a less-structured turn conformation; additionally, most of the helical conformation was of the more extended 3–10 helix type. These differences illustrate that different lipid environments affect melittin secondary structure.

Peptide-lipid interactions

To identify important motifs for melittin adsorption onto the PFOB-NEP surface, the interaction of melittin with the membrane lipids were analyzed in detail.

Density overlap between melittin and the phospholipid monolayer—Number density profiles of melittin and lipid groups were calculated and are illustrated in Figure 3. The density profile of the monolayer was centered at zero and the density profiles of other parts of lipids, peptide, water, and PFOB were placed with respect to that of the monolayer. Comparison of the two density profiles shows that the relative position and distribution of a melittin peptide within each monolayer was almost identical. However, an interesting

difference was observed in the tryptophan sidechain density (shown in orange dashed lines). In the PFOB-NEP, the peak of tryptophan density moved by approximately 0.6 nm into the interior of the monolayer and the tryptophan sidechain was buried as deeply as the methylene group of the oleoyl chain. In the control, the tryptophan density was much closer to the lipid headgroup. Because of the deep melittin membrane penetration, the tryptophan density only marginally overlapped with water density but significantly overlapped with the PFOB density.

Peptide membrane penetration—To further understand the different melittin interaction with the two membrane systems, we determined the relative positions of C_α carbons with respect to the mean depth of the lipid glycerol moiety (see Figure 4). The peptides in both systems were located in a deeper region of the monolayer than where they were initially positioned. In the control system, the N-terminal helical segment was more deeply buried than the C terminus or the C-terminal helical segment. Generally C_α penetration in the PFOB-NEP was not as deep as in the control. Despite their small magnitude, a Student's *t*-test revealed that most of the differences between the two systems were statistically significant. The attenuated penetration in the PFOB-NEP was more substantial in residues 6 to 13 of the N-terminal helical segment: the N-terminal helical segment did not penetrate into the monolayer as deeply as in the control.

Peptide-lipid contacts—To further clarify the contribution of individual lipid moieties in their interaction with the embedded melittin peptide, a contact map[24] was constructed to enumerate interactions between lipid groups and each residue of melittin (see Figure 5). If the distance between any atoms of one lipid moiety and any atoms of one melittin residue was shorter than the cutoff distance of 0.6 nm, its contact number was incremented by one for that specific match. Figure 5A and B show that melittin interactions with adjacent lipids were very similar between the two systems. As expected[8a], hydrophobic residues interacted with lipid tails while charged residues interacted with the phosphate group most frequently and then with ester groups. Most of the hydrophobic residues could interact, albeit at very low frequency, with the termini of lipid tails. The most extensive interactions were made by the charged residues at the C-terminus. The contact map also displayed another pattern: the contact of hydrophobic residues with the even-numbered lipid moieties (4, 6, 8, …, 14) was greater than with the odd-numbered ones (5, 7, 9,…, 13). This pattern indicates that melittin interacted preferentially with the oleoyl chain which is more flexible than the palmitoyl chain. Previous analyses showed that the two systems had relatively small differences. To illustrate these minor statistically significant differences, heat maps were created for contact differences (Figure 5C) and *t*-value differences (Figure 5D) at each position. In Figure 5C, red colors indicate more frequent contacts in the PFOB-NEP system, blue colors represent the opposite. The difference between the two systems is statistically significant, with a *p*-value of 0.05 if *t*-value is greater than 2.021 (orange to red) or *t*-value is smaller than −2.021 (light to dark blue); the area colored by either cyan, yellow or green is considered to be statistically indistinguishable in Figure 5D. The much wider area colored in blue colors in Figure 5C clearly shows that melittin had more extensive interactions with surrounding lipids in the control system, which was more pronounced at N-terminal side of the peptide. Finally, Figure 5C shows that residues 17–23 exhibited the most extensive variation between the two systems with the highest *t*-values.

Melittin tryptophan 19 structure

Local residue structure—More detailed structural analyses shown in Figures 1E and F reveal that Trp19 is implicated in critical differences in melittin interaction with neighboring lipids. Existence of a hydrogen bond was defined by two criteria: the distance between the donor and acceptor should be smaller than 0.33 nm and the angle (H-donor-acceptor)

smaller than 35°. In the PFOB-NEP system, the tryptophan sidechain formed a hydrogen bond with the carbonyl oxygen of Leu16. The hydrogen bond was formed at an early stage of PFOB-NEP simulation and maintained for approximately 90% of the 300 ns simulation; however, this particular hydrogen bond was not detected in the control simulation. By forming this hydrogen bond, the tryptophan sidechain could reside in a deeper hydrophobic region of the monolayer, which increases the probability of direct contact with bromine atom of PFOB molecules.

Distribution of PFOB bromine atoms around melittin Trp19—To test the probability of direct contact between the Trp19 side chain and the bromine atom of PFOB molecules, the radial distribution of the bromine atom around the tryptophan sidechain was determined for and averaged over each independent sub-sample. The result is plotted in Figure 6. Non-zero bromine density appeared as close as 0.3 nm, indicating direct contact between the two moieties. This direct contact is important for explaining the mechanism for experimentally observed tryptophan fluorescence quenching[5] and supports the validity of our modeled planar PFOB-NEP interface and melittin interactions at this interface.

Membrane structure

One of the hallmarks of melittin interaction with lipid bilayers has been its ability to alter the membrane macroscopic structure in dramatic ways[8b, 25]. We examined the effect of melittin on the membranes in our two systems through several analyses.

Monolayer structure—To assess the structural changes of the membranes, monolayer thickness was determined and compared between the PFOB-NEP and control systems in the presence and absence of melittin. Bilayer thickness is typically determined by the distance between the phosphate group of each leaflet;[26] however, this definition is not applicable to monolayers. Therefore, our comparisons among the simulated systems used a definition of monolayer thickness determined from the mean distance between the phosphate group and the terminal methyl group of the palmitoyl chain. Figure 7 shows that the lipid monolayers became slightly (less than 1 Å) thicker in the control system when the membrane contained melittin. However, the thickness of the monolayer of the PFOB-NEP system was not changed in the presence of melittin. Lack of membrane thinning in the control simulation is counterintuitive to the experimental observation that melittin thins membrane at concentrations below the critical level. [9]

Lipid tail ordering—To have a more detailed view of melittin influence on the membrane, lipid tail order parameters were determined, providing an indication of the mean conformation of lipids in a membrane. First, the order parameters were computed globally by averaging the order parameters of all the lipids in each monolayer. Figure 8 shows that lipid tail order was increased in the presence of melittin and the degree of increase was more substantial near the headgroup than near the lipid tails. Global order parameter changes indicated that melittin exhibited direct ordering effects that could be dependent on proximity to the peptide. To test this, the order parameters were computed as a function of distance from the embedded melittin (see Figure 9). The membrane was subdivided into four shells around the peptide with thicknesses of 0.9 nm. The thickness was empirically determined to have at least one lipid in each shell in any simulated systems. If the separation between the geometric center of a lipid and the geometric center of any melittin residue was closer than 0.9 nm, the lipid was assigned to the first shell. If the center of the geometric center of any other lipids was closer than 0.9 –nm from the lipids in the first shell, the lipid was assigned to the second shell. In the same manner, the lipids in the third shell were assigned, and all the unassigned lipids were assigned to the fourth shell. This assignment and the calculation

of order parameters were repeated for every snapshot; order parameters were averaged for each shell over the course of simulation.

Figure 9 shows melittin disordered lipid tails in the first shell, indicating that membrane thinning occurred at the immediate vicinity of melittin but beyond the first shell, lipid tail orders increased. In the fourth shell, where lipids should be least affected by melittin, the order parameter values were approaching those of the melittin-free membranes, indicating a convergence to “bulk” behavior away from the melittin. This figure also shows that the melittin lipid-ordering effect was weaker and decayed more quickly in the PFOB-NEP system than in the control bilayer.

Discussion

This study is focused on understanding how melittin peptides interact with phospholipid monolayer on the surface of perfluorocarbon-based nanoemulsion particles. In particular, this work examines the molecular details underlying the experimental observations that (1) high mole fractions of melittin do not disrupt PFC NEP monolayers and that (2) melittin tryptophan fluorescence is quenched upon binding to PFOB-NEPs. Molecular dynamics simulations were used to provide molecular-scale details addressing these observations.

Validity of the control simulations

The melittin concentration of 100:1 lipid:peptide in our control simulations is greater than its critical concentration of 62:1 lipid:peptide, below which the peptide starts to shift from a parallel to perpendicular orientation with respect to the membrane surface[9]. However, the 100:1 ratio is known to be sufficient to observe structural changes in both the peptide and membrane. [9]

The conformations of melittin and membrane structures in the control simulation showed good agreement with experimental observations. First, it is well known that helical conformations are predominant when melittin interacts with membrane due to its amphiphilicity.[27,28] Helical conformations of the peptide in the control bilayer were maintained throughout the simulations (Figure 2). Because of its more extensive hydrophobicity, the N-terminal helical segment is more deeply buried in the hydrophobic interior of membrane than the C-terminal segment,[29] as demonstrated in our control simulation (Figure 4). Experiments have shown that the melittin tryptophan side chain is located in the bilayer where the motions of the solvating water molecules of tryptophan side chain are restricted.[30] Our control simulation shows that tryptophan side chain resides at the lipid-water interface where water molecule motions are restricted due to abundant hydrogen-bond networks among interfacial water molecules and lipid head groups (Figure 3). Finally, melittin adsorption on the membrane surface thins the membrane until a critical melittin concentration is reached, beyond which additional melittin does not further decrease the membrane thickness.[9, 31] In our simulation, however, the membrane thinning effect was only observed in the direct vicinity of melittin peptides (Figure 9). Beyond this proximate region where lipids had direct interactions with the embedded melittin, membrane thickness was slightly increased. The same effect was observed in another study[32] and is likely due to finite size effects wherein lipids became more ordered to compensate the expansion due to disordered lipids near melittin peptides. Additionally, our simulations contain only 10 neutralizing chloride ions and therefore lacks the potential for counterion charge screening which may reduce the strength of interactions between highly positive melittin and surrounding zwitterionic lipid molecules. This hypothesis is supported by the observation that inclusion of counterions or removal of sidechain charges drastically delayed melittin adsorption onto membrane surface and loosened melittin interactions with the membrane.[32] However, overall, the control simulations showed that our simulation setup and force field

choices could provide us with reasonable structural details of melittin interactions with POPC membranes.

Resistance of PFOB-NEP monolayers to disruption by melittin

Membrane disruption by melittin peptides is known to occur via two distinct mechanisms depending on the lipid composition of the membrane. In one mechanism, melittin peptides make toroidal pores[9, 31, 3332, 34] in zwitterionic lipid membranes that mimic mammalian plasma membranes. In the other mechanism, melittin peptides can interact through carpet-like manner with membranes that contain high fractions of anionic lipids.[35] Different physicochemical properties are required for each mechanism. While strong positive charge is the most critical factor to determine disruption of anionic membranes via a carpet-like manner,[35] the binding and lytic activity of melittin to zwitterionic membranes via toroidal pores requires additional factors, including a long helical conformation and the presence of tryptophan residue.[9, 31, 33]

Our simulations showed that the interactions of melittin peptide with control bilayer and the PFOB-NEP monolayer were generally similar but included small statistically significant structural differences. First, the membrane penetration of the N-terminal helical segment and the overall helical content was reduced in the PFOB-NEP simulation (see Figure 4), which indicated less tightly bound melittin in the PFOB-NEP. Second, the tryptophan side chain was more deeply buried in the PFOB-NEP by forming a hydrogen bond with the carbonyl oxygen of Leu 16 (see Figure 1 and Figure 3). These differences may affect the lytic activity of melittin in zwitterionic membrane environments such as the PFOB-NEP egg lecithin monolayers.[5b,5a] However, our simulations contain only one peptide in each monolayer; therefore, additional simulations containing a more melittin peptides in each monolayer are necessary to draw more definite conclusions regarding lack of melittin-induced disruption of PFOB-NEP emulsifying monolayers.

A mechanism for melittin tryptophan fluorescence quenching in PFOB-NEPs

Previously, based on the observation that melittin tryptophan fluorescence could be quenched by water-soluble molecules, it had been argued that the melittin tryptophan should be located in the water-accessible region near the first carbon of the lipid tails of lipid bilayers.[27b] Indeed, in our control simulations, we observed that the tryptophan side chain maintains its position near the water-lipid interface where water-soluble quenching molecules have directly access. However, PFOB-NEPs have a unique intrinsic mechanism for quenching melittin tryptophan fluorescence.[5a] Our simulations provide a molecular-scale explanation for this experimentally observed quenching. In particular, the melittin tryptophan in the PFOB-NEP interface system resides in a deeper region of the lipid monolayer (see Figure 1) where direct contacts with the PFOB bromine are possible (see Figure 6), thus providing the interaction with bromine necessary for fluorescence quenching.[5a, 7]

Impact of PFOB on melittin binding to PFOB-NEPs

The phospholipid monolayer of perfluorocarbon based nanoemulsion particles (PFC NEP) is both important for emulsion stabilization as well as cargo binding. Perfluorocarbon molecules are both strongly hydrophobic as well as lipophobic as a result of strong electron negativity of fluorine atoms.[36] Therefore, unless cargo molecules are attached covalently to PFC NEPs, the phospholipid monolayer provides the only available region to bind both amphipathic (e.g. melittin peptide) and hydrophobic molecules.

We previously reported computational analyses which show that PFOB penetration into the emulsifying monolayer occurs, despite of the PFOB lipophobicity, due to the much shorter

length of PFOB (C8) compared to the fatty acyl chain of the phospholipids (C16, C18).[7, 37] PFOB intercalation between fatty acyl tails decreases the void volume but inversely increases packing density of the membrane. Increased packing density can be observed in the current simulations through higher order in the PFOB lipid tails as shown in Figure 8 and Figure 9. The penetration of PFOB into membrane void volumes reduces the space available for melittin and has significant potential for reducing binding affinity. Indeed, our simulations showed that the penetration of melittin into the PFOB-NEP monolayer was reduced compared to the peptide bound to the bilayer made of the same lipid.

These results indicate that the binding of cargo molecules may be affected by the intercalation of PFC molecules into the emulsifying monolayer, and such inhibitory effect is predicted to be larger for more hydrophobic cargo molecules that require deeper penetration into the monolayer. Several studies combining theoretical calculations and experimental measurements demonstrate the importance of hydrophobic interactions for loading and retaining of cargo molecules in drug formulations[38]. Hence, losing hydrophobic interactions with lipids could significantly affect the cargo loading and retention in the PFC NEPs. Therefore, it may be possible to improve PFC nanoemulsions by identifying additional PFC molecules with optimal levels of interaction with the emulsifying phospholipid monolayers that maximize the loading and retention of a cargo molecule of interest while maintaining the stability of the emulsion particles.

Conclusions

Our simulations revealed the molecular details of melittin bound to POPC bilayer and PFOB-NEP monolayer surfaces and rationalize the stability of the PFOB monolayers in the presence of melittin. Additionally, we provide an explanation of intrinsic PFOB-NEP tryptophan fluorescence quenching via direct collision of deeply buried Trp side chain and PFOB molecules inserted in between fatty acyl chains. Finally, our simulations demonstrate that the interaction of core-forming perfluorocarbon molecules with the emulsifying phospholipid monolayer can directly affect the mode of cargo binding to the perfluorocarbon-based nanoemulsion particles. Such analyses not only provide basic understanding of these unique materials but may also help to establish design principles for PFOB-NEPs that provide optimal combinations of emulsion stability and drug binding capability.

Supplementary Material

Refer to Web version on PubMed Central for supplementary material.

Acknowledgments

The authors thank Cornelia Brim for her help in the preparation of this manuscript. This work was sponsored by NIH grant R01 GM069702 to NAB, NIH grant U54 CA11934205 to SAW, NAB, and GML, and NIH grant U01 NS073457-01 to NAB and GML. Computational resources were provided by the Texas Advanced Computing Center through Teragrid Grants TG-MCB060053 and TG-MCA08X003 as well as the National Biomedical Computation Resource (NIH P41 RR0860516).

References

1. (a) Wagner V, Dullaart A, Bock AK, Zweck A. The emerging nanomedicine landscape. Nature Biotechnology. 2006; 24(10):1211–1217.(b) Krafft MP. Fluorocarbons and fluorinated amphiphiles in drug delivery and biomedical research. Adv Drug Deliver Rev. 2001; 47(2–3):209–228.(c) Zhou, Z-x; Zhang, B-g; Zhang, H.; Huang, X-z; Hu, Y-l; Sun, L.; Wang, X-m; Zhang, J-w. Drug packaging and delivery using perfluorocarbon nanoparticles for targeted inhibition of vascular smooth muscle cells. Acta Pharmacologica Sinica. 2009; 30(11):1577–1584. [PubMed: 19890365]

(d) Pan D, Lanza GM, Wickline SA, Caruthers SD. Nanomedicine: perspective and promises with ligand-directed molecular imaging. Eur J Radiol. 2009; 70(2):274–285. [PubMed: 19268515]

2. Kuznetsova IN. Perfluorocarbon Emulsions: Stability in vitro and in vivo (A Review). Pharmaceutical Chemistry Journal. 2003; 37(8):415–420.
3. Riessa JG, Krafft MP. Fluorinated materials for in vivo oxygen transport (blood substitutes), diagnosis and drug delivery. Biomaterials. 1998; 19(16):1529–1539. [PubMed: 9794531]
4. (a) Chang, T. Red Blood Cell Substitutes: Past, Present, and Future. Kobayashi, K.; Tsuchida, E.; Horinouchi, H., editors. Vol. 12. Springer; 2005. p. 22-33.(b) Gerber F, Krafft MP, Vandamme TF, Goldmann M, Fontaine P. Fluidization of a Dipalmitoyl Phosphatidylcholine Monolayer by Fluorocarbon Gases: Potential Use in Lung Surfactant Therapy. Biophys J. 2006; 90(9):3184–3192. [PubMed: 16500985]
5. (a) Soman NR, Lanza GM, Heuser JM, Schlesinger PH, Wickline SA. Synthesis and Characterization of Stable Fluorocarbon Nanostructures as Drug Delivery Vehicles for Cytolytic Peptides. Nano Lett. 2008; 8(4):1131–1136. [PubMed: 18302330] (b) Soman NR, Baldwin SL, Hu G, Marsh JN, Lanza GM, Heuser JE, Arbeit JM, Wickline SA, Schlesinger PH. Molecularly targeted nanocarriers deliver the cytolytic peptide melittin specifically to tumor cells in mice, reducing tumor growth. J Clin Invest. 2009; 119(9):2830–2842. [PubMed: 19726870]
6. Lavignac N, Lazenby M, Franchini J, Ferruti P, Duncan R. Synthesis and preliminary evaluation of poly(amidoamine)-melittin conjugates as endosomolytic polymers and/or potential anticancer therapeutics. International Journal of Pharmaceutics. 2005; 300(1–2):102–112. [PubMed: 16009513]
7. Lee S-J, Olsen B, Schlesinger PH, Baker NA. Characterization of Perfluorooctylbromide-Based Nanoemulsion Particles Using Atomistic Molecular Dynamics Simulations. The Journal of Physical Chemistry B. 2010; 114(31):10086–10096. [PubMed: 20684632]
8. (a) Dempsey C. The actions of melittin on membranes. Biochimica et Biophysica Acta (BBA) - Reviews on Biomembranes. 1990; 1031(2):143–161.(b) Hristova K, Dempsey CE, White SH. Structure, Location, and Lipid Perturbations of Melittin at the Membrane Interface. Biophys J. 2001; 80(2):801–811. [PubMed: 11159447]
9. Lee M-T, Chen F-Y, Huang HW. Energetics of Pore Formation Induced by Membrane Active Peptidesdag. Biochemistry. 2004; 43(12):3590–3599. [PubMed: 15035629]
10. Berger O, Edholm O, Jahnig F. Molecular dynamics simulations of a fluid bilayer of dipalmitoylphosphatidylcholine at full hydration, constant pressure, and constant temperature. Biophysical Journal. 1997; 72(5):2002–2013. [PubMed: 9129804]
11. Chiu S-W, Clark MM, Balaji V, Subramaniam S, Scott HL, Jakobsson E. Incorporation of surface tension into molecular dynamics simulation of an interface: a fluid phase lipid bilayer membrane. Biophys J. 1995; 69(4):1230–1245. [PubMed: 8534794]
12. Berendsen, HJC.; Postma, JPM.; van Gunsteren, WF.; Hermans, J. INTERACTION MODELS FOR WATER IN RELATION TO PROTEIN HYDRATION. Pullman, B., editor. D. Reidel Publishing Company; 1981. p. 331-342.
13. Kaminski GA, Friesner RA, Tirado-Rives J, Jorgensen WL. Evaluation and Reparametrization of the OPLS-AA Force Field for Proteins via Comparison with Accurate Quantum Chemical Calculations on Peptides. J Phys Chem B. 2001; 105(28):6474–6487.
14. Chakrabarti N, Neale C, Payandeh J, Pai EF, Pomès Rg. An Iris-Like Mechanism of Pore Dilation in the CorA Magnesium Transport System. Biophys J. 2010; 98(5):784–792. [PubMed: 20197031]
15. Hess B, Kutzner C, van der Spoel D, Lindahl E. GROMACS 4: Algorithms for Highly Efficient, Load-Balanced, and Scalable Molecular Simulation. J Chem Theory Comput. 2008; 4(3):435–447.
16. Lee S-J, Song Y, Baker NA. Molecular dynamics simulations of asymmetric NaCl and KCl solutions separated by phosphatidylcholine bilayers: potential drops and structural changes induced by strong Na+-lipid interactions and finite size effects. Biophys J. 2008; 94(9):3565–3576. [PubMed: 18222999]
17. Darden T, York D, Pedersen L. Particle mesh Ewald: An N [center-dot] log(N) method for Ewald sums in large systems. J Chem Phys. 1993; 98(12):10089–10092.
18. Parrinello M, Rahman A. Polymorphic transitions in single crystals: A new molecular dynamics method. J Appl Phys. 1981; 52(12):7182–7190.

19. Hoover WG. Canonical dynamics: Equilibrium phase-space distributions. Phys Rev A. 1985; 31(3):1695–1697. [PubMed: 9895674]
20. Hess B, Bekker H, Berendsen HJC, Fraaije JGEM. LINCS: A linear constraint solver for molecular simulations. J Comput Chem. 1997; 18(12):1463–1472.
21. Grossfield A, Zuckerman DM. Chapter 2 Quantifying Uncertainty and Sampling Quality in Biomolecular Simulations. Annu Rep Comput Chem. 2009; 5:23–48. [PubMed: 20454547]
22. (a) Raghuraman H, Chattopadhyay A. Influence of lipid chain unsaturation on membrane-bound melittin: a fluorescence approach. Biochimica et Biophysica Acta (BBA) -Biomembranes. 2004; 1665(1–2):29–39.(b) Shai Y. Mechanism of the binding, insertion and destabilization of phospholipid bilayer membranes by a-helical antimicrobial and cell non-selective membrane-lytic peptides. Biochimca et Biophysica Acta. 1999; 1462:55–70.
23. Kabsch W, Sander C. Dictionary of protein secondary structure: Pattern recognition of hydrogen-bonded and geometrical features. Biopolymers. 1983; 22(12):2577–2637. [PubMed: 6667333]
24. Tran H, Pappu R. Toward an Accurate Theoretical Framework for Describing Ensembles for Proteins under Strongly Denaturing Conditions. Biophys J. 2006; 91(5):1868–1886. [PubMed: 16766618]
25. (a) Chen FY, Lee MT, Huang HW. Evidence for Membrane Thinning Effect as the Mechanism for Peptide-Induced Pore Formation. Biophysical Journal. 2003; 84(6):3751–3758. [PubMed: 12770881] (b) Lee MT, Hung WC, Chen FY, Huang HW. Mechanism and kinetics of pore formation in membranes by water-soluble amphipathic peptides. Proceedings of the National Academy of Sciences. 2008; 105(13):5087–5092.
26. Kucerka N, Tristram-Nagle S, Nagle J. Structure of Fully Hydrated Fluid Phase Lipid Bilayers with Monounsaturated Chains. Journal of Membrane Biology. 2006; 208(3):193. [PubMed: 16604469]
27. (a) Ladokhin AS, White SH. Folding of amphipathic α-helices on membranes: energetics of helix formation by melittin. J Mol Biol. 1998; (29):7.(b) Vogel H, Jahnig F. The structure of melittin in membranes. Biophysical Journal. 1986; 50(4):573–582. [PubMed: 3779000]
28. Raghuraman H, Chattopadhyay A. Melittin: a Membrane-active Peptide with Diverse Functions. Bioscience Reports. 2007; 27(4):35.
29. Brauner JW, Mendelsohn R, Prendergast FG. Attenuated Total Reflectance Fourier Transform Infrared Studies of the Interaction of Melittin, Two Fragments of Melittin, and δ-Hemolysin with Phosphotidylcholines. Biochemistry. 1987; 26:8.
30. Chattopadhyay A, Rukmini R. Restricted mobility of the sole tryptophan in membrane-bound melittin. FEBS Lett. 1993; 335(3):4.
31. Huang H. Molecular mechanism of antimicrobial peptides: The origin of cooperativity. Biochimica et Biophysica Acta (BBA) - Biomembranes. 2006; 1758(9):1292–1302.
32. Sengupta D, Leontiadou H, Mark AE, Marrink S-J. Toroidal pores formed by anitimicrobial peptides show significant disorder. Biochimica et Biophysica Acta (BBA) -Biomembranes. 2008; 1778(10):10.
33. (a) Yang L, Harroun TA, Ding L, Huang HW. Barrel-Stave Model or Toroidal Model? A Case Study on Melittin Pores. Biophys J. 2001; 81(3):35.(b) Allende D, Simon SA, McIntosh TJ. Melittin-Induced Bilayer Leakage Depends on Lipid Material Properties: Evidence for Toroidal Pores. Biophys J. 2005; 88(3):10.
34. Rzepiela AJ, Sengupta D, Goga N, Marrink SJ. Membrane poration by antimicrobial peptides combining atomistic and coarse-grained descriptions. Faraday Discuss. 2010; 144:13.
35. (a) Pouny Y, Shai Y. Interaction of D-amino acid incorporated analogs of pardaxin with membranes. Biochemistry. 1992; 31(39):9.(b) Shai Y. Mechanism of the binding, insertion and destabilization of phospholipid bilayer membranes by a-helical antimicrobial and cell non-selective membrane-lytic peptides. BBA. 1999; 1462:16.(c) Ladokhin AS, White SH. ‘Detergent-like’ permeabilization of anionic lipid vesicles by melittin. BBA-Biomembranes. 2001; 1514(2):8.
36. (a) Lemal DM. Perspective on Fluorocarbon Chemistry. J Org Chem. 2004; 69(1):11.(b) KANEDA MM, CARUTHERS S, LANZA GM, WICKLINE SA. Perfluorocarbon Nanoemulsions for Quantitative Molecular Imaging and Targeted Therapeutics. Ann Biomed Eng. 2009; 37(10):12.

37. Yokoyama H, Nakahara H, Shibata O. Miscibility and phase behavior of DPPG and perfluorocarboxylic acids at the air–water interface. Chem Phys Lipids. 2009; 161(2):11. [PubMed: 19559016]

38. (a) Loan Huynh JG, Leroux J-C, Delmas P, Allen C. Predicting the Solubility of the Anti-Cancer Agent Docetaxel in Small Molecule Excipients using Computational Methods. Pharm Res. 2008; 25(1):11.(b) Costache AD, Sheihet L, Zaveri K, Knight DD, Kohn J. Polymer-Drug Interactions in Tyrosine-Derived Triblock Copolymer Nanospheres: A Computational Modeling Approach. Mol Pharmaceutics. 2009; 6(5):8.

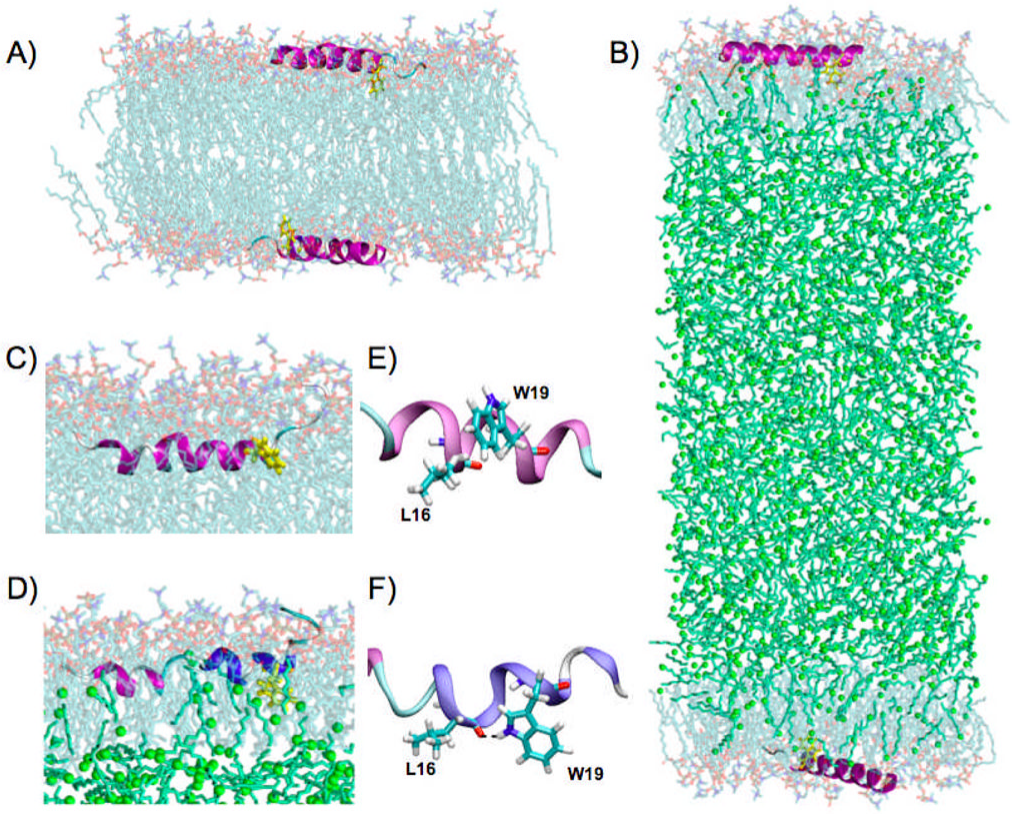

Figure 1.
Structures of melittin bound to membranes. Initial structures of the (A) control and (B) PFOB-NEP systems. Melittin in a monolayer of the (C) control and (D) PFOB-NEP at approximately 300 ns. Representative conformations of L16 and W19 in the (E) Control and (F) PFOB-NEP. Phosphatidylcholine lipids are shown in cyan for carbon, blue for nitrogen, gold for phosphorus, red for oxygen atoms. PFOB is shown in green sticks with an explicit bromine atom depicted as a green ball. The peptides are shown in ribbon style with an explicit tryptophan sidechain in yellow (A,B,C,D). Each residue is colored based on their secondary structure: α helix in magenta, 3–10 helix in blue, turns in cyan, and random coil in white.

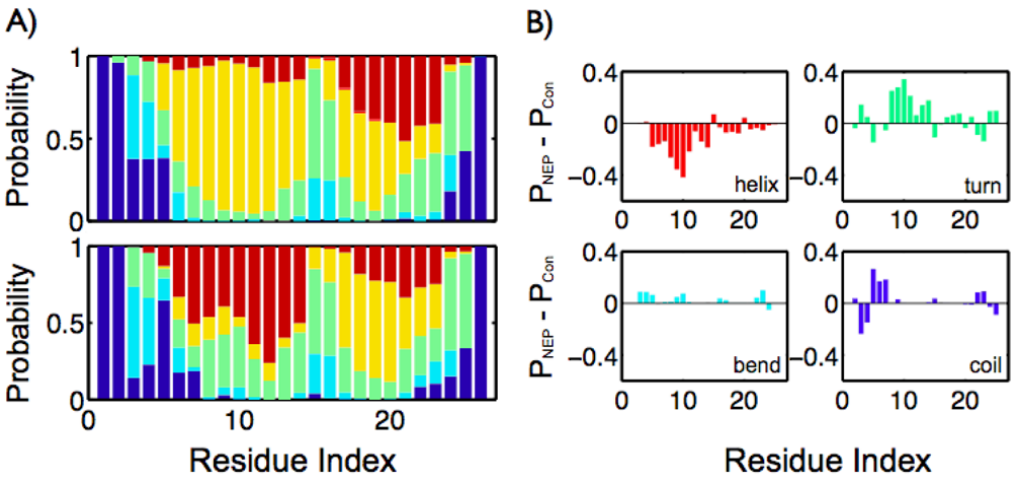

Figure 2.

The secondary structure content of each melittin residue. (A) The top panel shows the secondary structure contents of the control, the bottom shows those of the PFOB-NEP system. The secondary structures were categorized random-coil (blue), bend (cyan), turn (green), alpha-helix (yellow), 5-helix (light red), and 3–10 helix (dark red). (B) The difference in the content for each conformation between the control and PFOB-NEP system is plotted individually. The three different helical conformations were combined as an alpha-helix in this calculation.

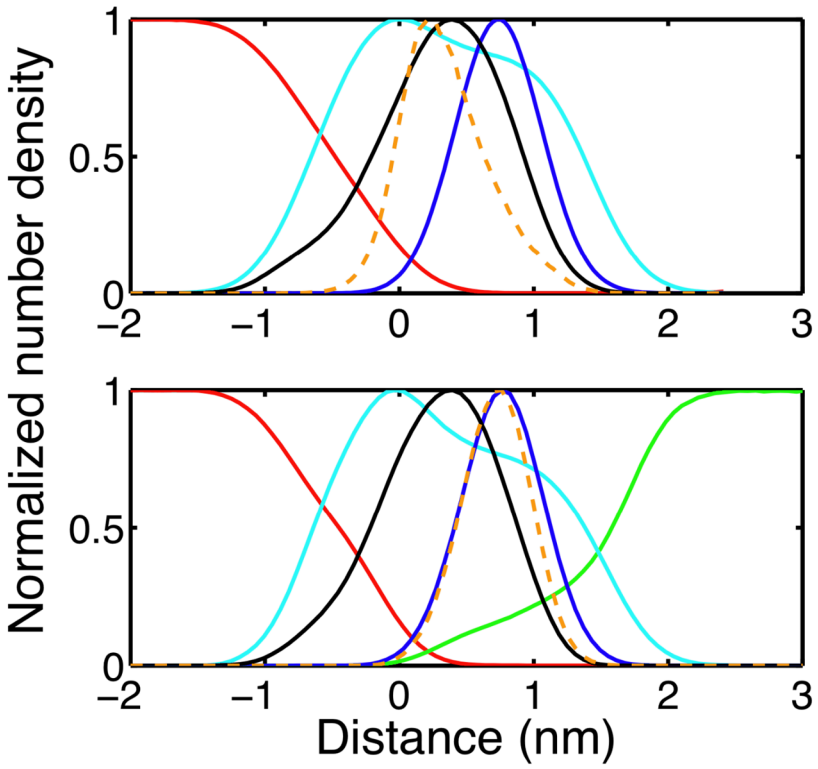

Figure 3.
Number density profiles of the phospholipid monolayer and embedded melittin peptide for the control (top) and PFOB-NEP (bottom) systems. The density of the monolayer is shown in cyan and the density of methylene group in blue. The density of the entire melittin peptide is shown in black and that of tryptophan sidechain (W19) is shown in an orange dashed line. The density of water is shown in red and PFOB (only in the bottom panel) in green.

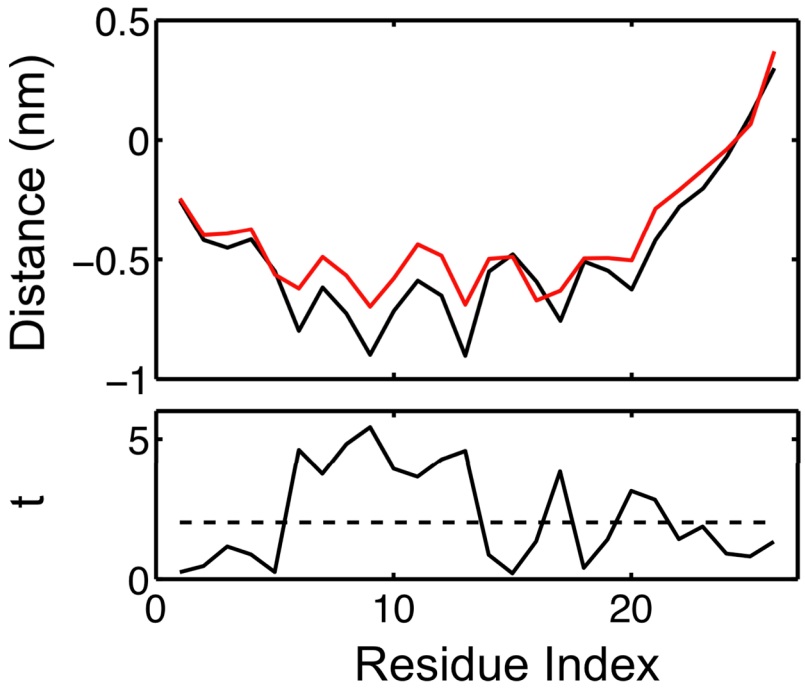

Figure 4.

Penetration of melittin into the phospholipid monolayer. The top panel shows the relative mean positions of Cα carbons of the control (black) and the PFOB-NEP (red) systems with respect to the position of the lipid glycerol groups of each monolayer. A positive value indicates that a Cα carbon locates near the surface of monolayer while negative value indicates that a Cα carbon locates in the hydrophobic interior of monolayer. The bottom panel shows the student t-values for differences in Cα positions between the control and PFOB-NEP systems. The dashed black line indicates the t-value (n = 48) for a significant difference at a 95 percent confidence level. The n number is doubled since two data sets (one for each monolayer) were obtained from each block.

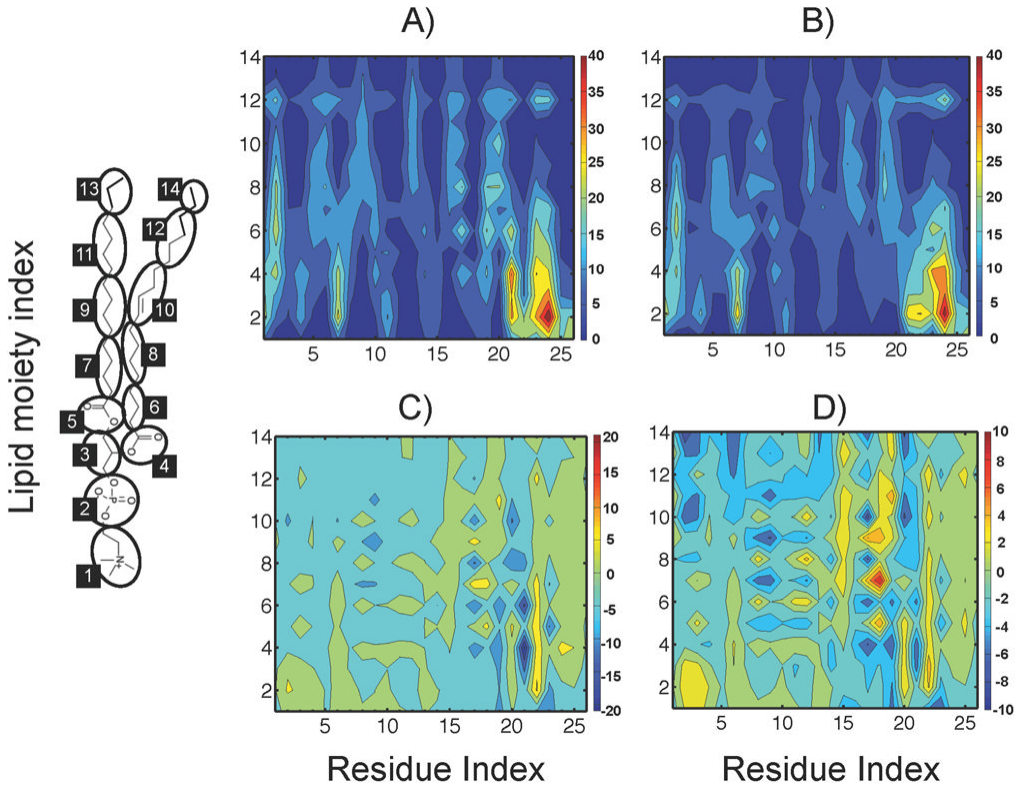

Figure 5.

The contact map between residues of the peptide and the lipid groups illustrated on the left. The lipid-melittin contacts in the (A) control (B) PFOB-NEP systems are shown by contour maps. The difference in contact number between the two systems is shown (C) and t-values for the difference are plotted in (D). Smaller indices indicate lipid moieties closer to the hydrophilic surface while larger indices indicate moieties that are deeper in the hydrophobic core. Please refer to the text for additional details about each panel.

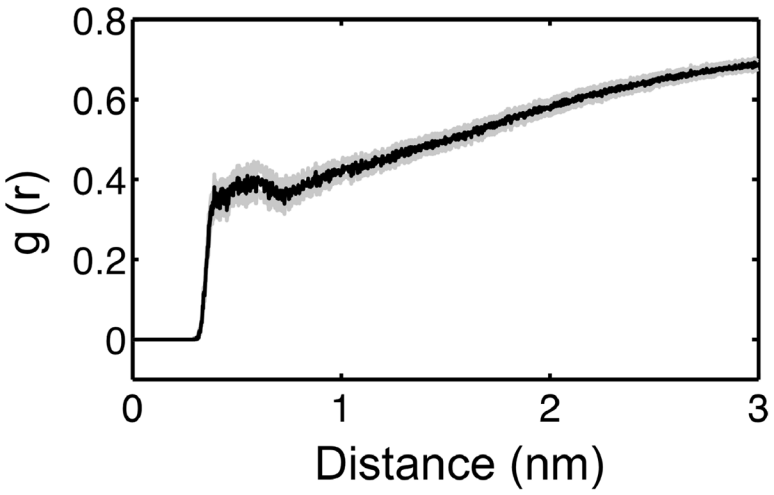

Figure 6.
Radial distribution function of the bromine atom of PFOB around the tryptophan (W19) side chain. The black solid line shows the mean of the distribution and the gray solid lines show the one standard error deviation of the distribution.

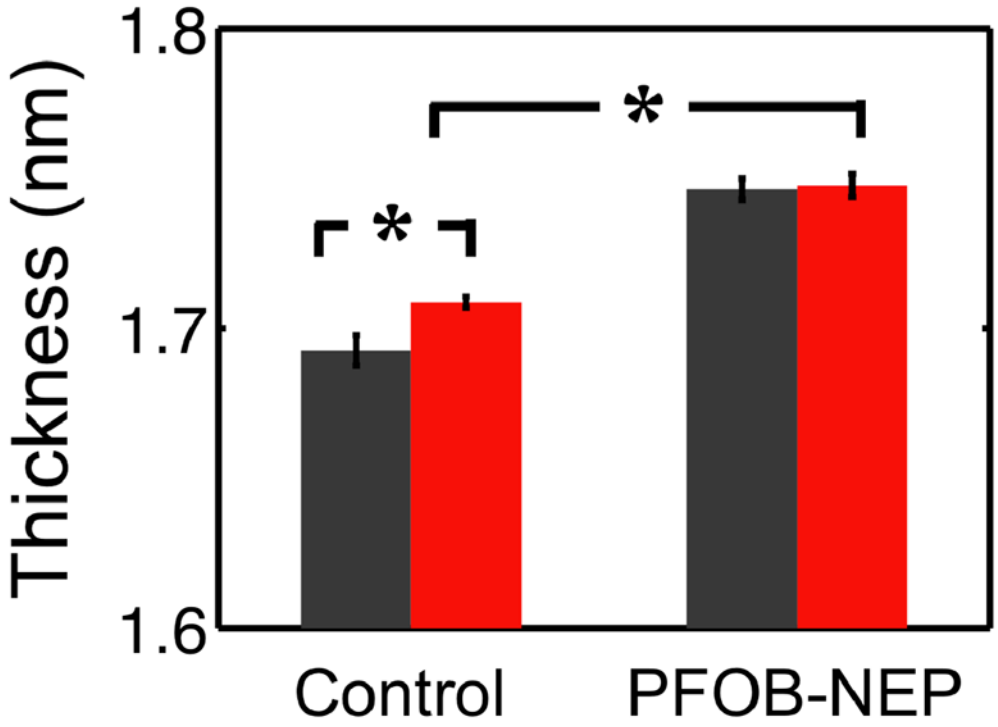

Figure 7.
The thickness of the monolayer of the control and the PFOB-NEP. The graphs represent the mean distance between the phosphate and the terminal methyl of the palmitoyl chain in our equilibrated simulation. Dark gray bars are for the unperturbed monolayers while red bars indicate the melittin-containing system. The * symbol indicates statistically significant differences with a *p*-value of 0.05.

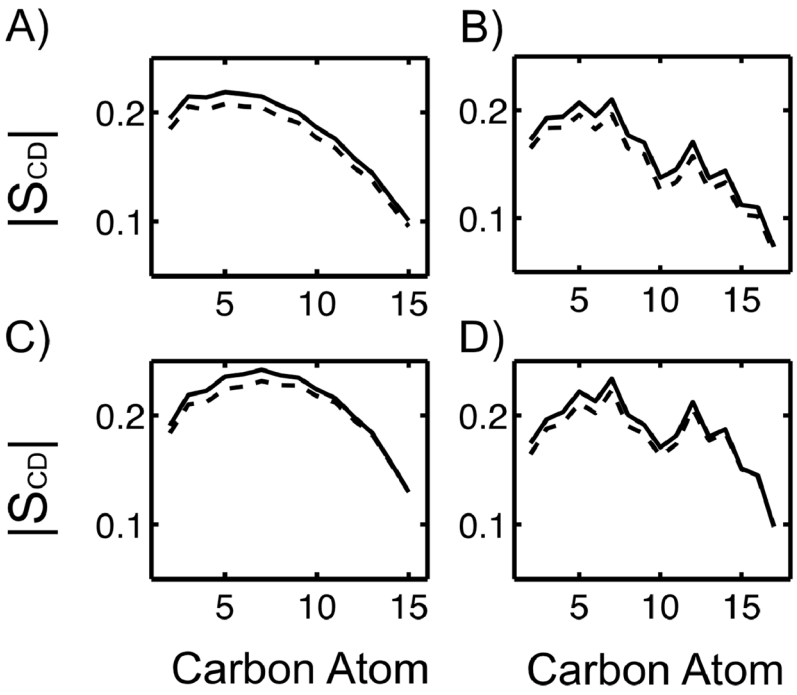

Figure 8.
Lipid order parameters averaged over all lipids in each monolayer. The deuterium order parameters of the palmitoyl chain (left panels) and the oleoyl chain (right panels) of the control (top panels) and the PFOB-NEP (bottom panels) systems. Data from systems containing melittin peptides are shown in solid black lines; the dashed black lines are the order parameters of the same membranes but in the absence of melittin.

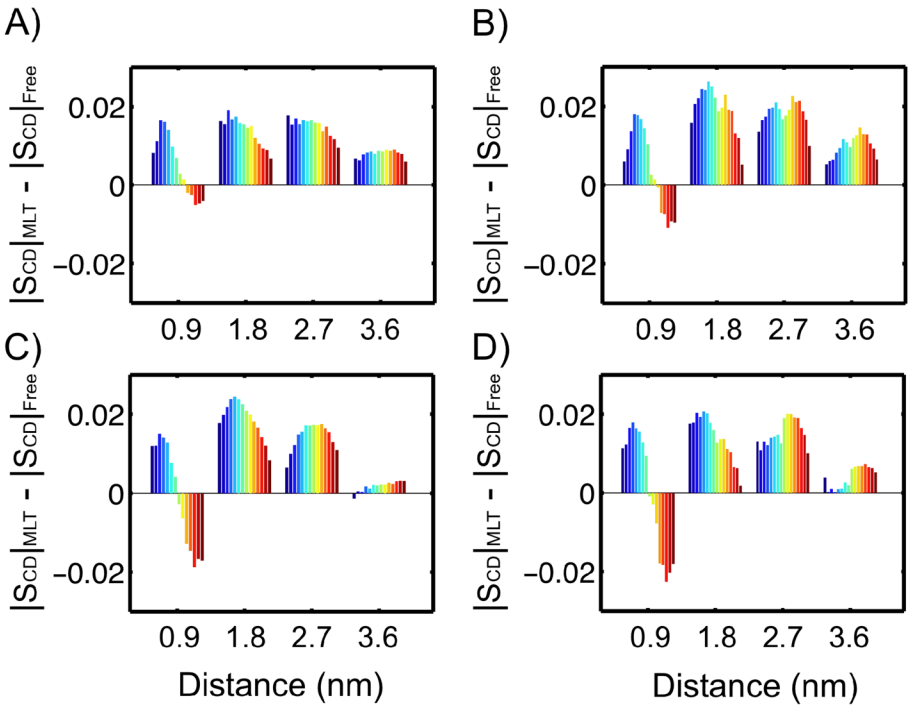

Figure 9.

Differences in the order parameters in the presence and in the absence of melittin as a function of lipid distance from the melittin. The differences of the palmitoyl chain (left panels) and the oleoyl chain (right panels) of the control (top panels) and the PFOB-NEP (bottom panels) systems are plotted separately. The narrow bars profile the difference in the order parameter of each carbon bond. The palmitoyl chain has 14 carbon bonds and the oeloyl chain has 16 bonds. The bonds near the polar head group are colored in blue and those near the hydrophobic tail end in dark red.